Poly(ethylene oxide)-co-Poly(propylene oxide)-Based Gel Electrolyte with High Ionic Conductivity and Mechanical Integrity for Lithium-Ion Batteries

Shih-Hong Wang,[†] Sheng-Shu Hou,[†] Ping-Lin Kuo,[†] and Hsisheng Teng*[,†,‡]

[†]Department of Chemical Engineering and Research Center for Energy Technology and Strategy, National Cheng Kung University, Tainan 70101, Taiwan

[‡]Center for Micro/Nano Science and Technology, National Cheng Kung University, Tainan 70101, Taiwan

Ⓢ Supporting Information

ABSTRACT: Using gel polymer electrolytes (GPEs) for lithium-ion batteries usually encounters the drawback of poor mechanical integrity of the GPEs. This study demonstrates the outstanding performance of a GPE consisting of a commercial membrane (Celgard) incorporated with a poly(ethylene oxide)-co-poly(propylene oxide) copolymer (P(EO-co-PO)) swelled by a liquid electrolyte (LE) of 1 M $LiPF_6$ in carbonate solvents. The proposed GPE stably holds LE with an amount

that is three times that of the Celgard-P(EO-co-PO) composite. This GPE has a higher ionic conductivity (2.8×10^{-3} and 5.1×10^{-4} S cm^{-1} at 30 and -20 °C, respectively) and a wider electrochemical voltage range (5.1 V) than the LE-swelled Celgard because of the strong ion-solvation power of P(EO-co-PO). The active ion-solvation role of P(EO-co-PO) also suppresses the formation of the solid−electrolyte interphase layer. When assembling the GPE in a Li/LiFePO$_4$ battery, the P(EO-co-PO) network hinders anionic transport, producing a high Li$^+$ transference number of 0.5 and decreased the polarization overpotential. The Li/GPE/LiFePO$_4$ battery delivers a discharge capacity of 156−135 mAh g^{-1} between 0.1 and 1 C-rates, which is approximately 5% higher than that of the Li/LE/LiFePO$_4$ battery. The IR drop of the Li/GPE/LiFePO$_4$ battery was 44% smaller than that of the Li/LE/LiFePO$_4$. The Li/GPE/LiFePO$_4$ battery is more stable, with only a 1.2% capacity decay for 150 galvanostatic charge−discharge cycles. The advantages of the proposed GPE are its high stability, conductivity, Li$^+$ transference number, and mechanical integrity, which allow for the assembly of GPE-based batteries readily scalable to industrial levels.

KEYWORDS: gel electrolyte, lithium-ion battery, ionic conductivity
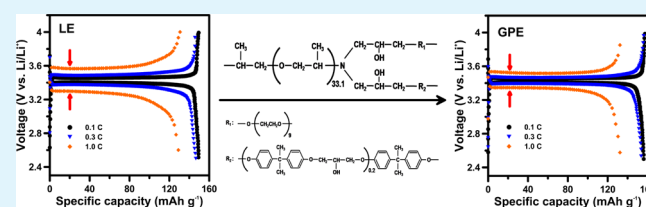
1. INTRODUCTION

Electrochemical devices that store energy (such as lithium-ion batteries or supercapacitors) and convert energy (such as dye-sensitized solar cells) are mainly composed of an electrolyte solution and two facing electrodes separated by a film.[1−7] The electrolyte used affects the stability and active voltage ranges of the device. The leakage or evaporation of solvent from the electrolyte solution limits the long-term stability of electrochemical devices. Rechargeable lithium-ion batteries that use polymer electrolytes instead of conventional liquid electrolytes are suitable for various geometries because they are leak proof and easily fabricated into the desired shapes and sizes.[8] Solid polymer electrolyte applications are limited because of their relatively low conductivity at low temperatures, poor contact at the electrode/electrolyte interface, and low solubility of lithium salts in polymer matrices.[9−11] Gel polymer electrolytes (GPEs), which consist of a polymeric framework, solvent (plasticizer), and supporting electrolytic salt, show acceptable ionic conductivity over a wide temperature range for lithium-ion polymer batteries.[12] However, a thin GPE film with low ionic resistance generally lacks two key properties of solids, mechanical integrity and persistent structure, that are essential

for facile cell assembly. Reinforcing GPE films with filler to improve mechanical and other properties, such as operating safety,[13,14] is critical for practical GPE applications.

Host polymers used for GPE preparation include poly(ethylene oxide) (PEO),[15] poly(vinylidene fluoride) (PVdF),[16,17] poly(vinylidene fluoride-co-hexaflouropropylene) (P(VdF-HFP)),[18−20] poly(urethane) (PU),[21] poly(acrylonitrile) (PAN),[22] and poly(methyl methacrylate) (PMMA).[23−25] Table 1 shows a performance summary of Li/LiFePO$_4$ batteries assembled with GPEs of various compositions.[20−22,26−35] In most cases, the batteries either had relatively low capacities (<150 mAh g^{-1}) or exhibited poor capacity retention with cycling. How effectively the polymers can dissociate the supporting electrolytic salts and/or trap plasticizer solvent molecules by solvation governs the performance of GPE-based batteries. Ion transport by segmental polymer-chain motion is not sufficiently efficient to compensate for the transport interference caused by the polymer frame-

Table 1. Electrochemical Performance of GPEs Consisting of Different Polymeric Frameworks and Supporting Electrolytes: The Capacity of the Resulting Li/LiFePO₄ Batteries and Resistance at the Li/GPE Interface

GPE composition (polymer/electrolyte)[a]	Li/LiFePO$_4$ cell capacity (mAh g^{-1})	capacity retention (%)	Li/GPE interface resistance (Ω)	ref
PVdF-PU/LiClO$_4$-EC-PC	169 (0.1 C)	84 (50 cycles at 0.1 C)		21
PAN/LiPF$_6$-EC-DMC	150 (0.1 C)	90 (50 cycles at 0.1 C)		22
PVC-PMMA/LiPF$_6$-EC-DMC		99 (100 cycles at 0.5 C with graphite/LiCoO$_2$)	31	25
PEO/LiTFSI-BMITFSI	140 (0.1 C)		3547	26
PVdF/LiClO$_4$-EC-PC-Al$_2$O$_3$	150 (0.2 C)		~650	27
PVdF-PVC/LiClO$_4$-EC-PC	145 (0.1 C)	90 (50 cycles at 0.1 C)		28
PVdF-PMMA/LiPF$_6$-EC-DMC	135 (0.05 C)	99 (50 cycles at 0.05 C)		29
P(VdF-HFP)-PAN/LiPF$_6$-EC-DMC	145 (0.1 C)	94 (50 cycles at 0.1 C)	~240	30
PAN-PMMA/PYR$_{14}$TFSI-LiTFSI		92 (50 cycles at 0.2 C)	~280	31
P(AN-MMA-VAc)/PYR$_{14}$TFSI-LiTFSI-VC	142 (0.1 C)	99 (50 cycles at 0.1 C)	48	32
P(VdF-HFP)/PYRA$_{1201}$TFSI-LiTFSI-SiO$_2$	139 (0.1 C)	84 (174 cycles at 0.2 C)	118	20
P(VdF-HFP)/PP$_{14}$TFSI-LiTFSI	159 (1 C)	69 (60 cycles at 1 C)	~380	33
P(VdF-HFP)/1g13TFSI-LiTFSI	142 (0.1 C)	100 (100 cycles at 0.1 C)	62	34
P(VdF-HFP)/PY$_{24}$LiTFSI-BMITFSI-EC-PC	149 (0.1 C)		~500	35
Celgard-P(EO-PO)/LiPF$_6$-EC-DEC-DMC	156 (0.1 C)	99 (150 cycles at 0.5 C)	7−15	this work

[a]PC, propylene carbonate; EMC, ethyl methyl carbonate; VC, vinylene carbonate; PS, polystyrene; PVC, poly(vinyl chloride); LiTFSI, lithium bis(trifluoromethanesulfonyl)imide; BMITFSI, 1-butyl-3-methylimidazolium bis(trifluoromethanesulfonyl)imide; PYR$_{14}$TFSI, N-methy-N-butylpyrrolidinium bis(trifluoromethanesulfonyl)imide; PYRA$_{1201}$TFSI, N-ethyl(methylether)-N-methylpyrrolidinium trifluoromethanesulfonimide; PP14TFSI, N-methyl-N-butylpiperidiniumbis(trifluoromethanesulfonyl)imide; 1g13TFSI, guanidinium-based salts; and Py$_{24}$TFSI, N-n-butyl-N-ethylpyrrolidinium N,N-bis(trifluoromethane)sulfonimide.

work. The polymer functionalities must have the ability to solvate the ions for the enhanced salt dissociation that results in high storage capacity and ionic conductivity. In addition, the ability to immobilize anions for a higher lithium-ion transference number (t_{Li+}) during ion transport has to be taken into account.

Among various functional polymers, PEO chains are an important component of GPE polymeric frameworks because they effectively solvate electrolytic ions and serve as a solvent gelator.[36] In practice, modifying PEO with other polymers is essential for reducing the crystallinity that retards ion motion in the polymeric framework. The incorporation of PEO with poly(propylene oxide) (PPO), which is structurally compatible with PEO, reduces the tendency of a PEO-based polymeric framework to crystallize and creates volume for ion motion.[37,38] The strong dipole moment of the poly(ethylene oxide)-co-poly(propylene oxide) (P(EO-co-PO)) copolymer holds solvent molecules and avoids solvent leakage and evaporation. However, solvent swelling reduces the mechanical strength of the P(EO-co-PO) network.

Poly(propylene) (PP) is a suitable separator material for liquid-electrolyte lithium-ion batteries because PP fabric has mechanical integrity and is compatible with organic solvents. Commercially available separator membranes contain PP fabric and have a regulated thickness. The solvents swell the membranes by segregating the polymeric chains and allow the transport of electrolyte ions through the film. By taking advantage of the mechanical integrity and regulated thickness of a commercial PP-containing separator, GPEs incorporated with a PP-separator membrane can have reinforced mechanical integrity for materials processing and a well-controlled film thickness. The gel-forming function of GPEs also modifies the separator to encapsulate the electrolyte solution, further

assisting in adhering the electrodes to the separator for easy battery assembly.[39]

This study synthesizes a composite by incorporating a P(EO-co-PO) copolymer with a commercially available trilayer PP/polyethylene (PE)/PP membrane (Celgard M824), called Celgard, to form a framework for a composite GPE. The P(EO-co-PO) matrices, which are reinforced by blending with diglycidyl ether of bisphenol A (DGEBA), effectively dissociate the lithium salt and enclose sufficient solvent molecules to facilitate ionic transport in the solvent channels. The P(EO-co-PO) chains also segregate the Celgard polymer chains for better polymer plasticization with the solvent. The composite GPE, Celgard-P(EO-co-PO), has an ionic conductivity of approximately 10^{-3} S cm^{-1} at room temperature and excellent mechanical integrity. In comparison with the previous results shown in Table 1, a Li/LiFePO$_4$ battery assembled with Celgard-P(EO-co-PO) shows superior performance with both a high storage capacity and long cycle life. In addition, the high solvation ability and good electrode/electrolyte compatibility extends the battery voltage range and promotes the energy-storage performance. This GPE can be synthesized at an industrial scale, and its mechanical integrity enables roll-to-roll battery assembly.

2. EXPERIMENTAL SECTION

2.1. Preparation of the Composite Celgard-P(EO-co-PO) Membrane. The P(EO-co-PO) copolymer was prepared from poly(ethylene glycol) diglycidyl ether (PEGDE) with poly(propylene oxide) diamines as a curing agent. DGEBA was blended with the polymer precursors before curing to improve the mechanical properties. PEGDE (Kyoeisha) and DGEBA (Nan-Ya) with epoxy group equivalent weights of 290 and 190 g^{-1}, respectively, and a curing agent, α,ω-diamino poly(propylene oxide) (Huntsman Jeffamine D2000) with an active hydrogen equivalent weight of 514 g^{-1}, constituted the polymeric framework of the gel electrolyte. The

8478

dx.doi.org/10.1021/am4019115 | ACS Appl. Mater. Interfaces 2013, 5, 8477−8485

preparation of this polymer was initiated by dissolving 0.1 g of PEGDE, 0.1 g of DGEBA, and 0.45 g of D2000 in 0.1 mL of ethylene glycol and 0.5 mL of ethanol by mechanical stirring to form a polymer precursor solution. The precursor compositions used in the present study resulted in a durable polymer framework that effectively absorbed electrolyte solutions. The trilayer Celgard membrane was impregnated with the polymer precursor solution, and the membrane was heat treated at 40 °C for 24 h to cure the impregnated polymer. The resulting Celgard-P(EO-co-PO) film, with a P(EO-co-PO)-to-Celgard ratio of 0.8, was 20 μm thick, flexible, and transparent. The Celgard-P(EO-co-PO) film was soaked in an electrolyte solution of 1 M LiPF$_6$ dissolved in ethylene carbonate/dimethyl carbonate/diethyl carbonate (EC/DMC/DEC) (1:1:1 by volume) for 12 h to trap the solution in the polymer network to form the GPE film. The mass ratio of the trapped solution to the Celgard-P(EO-co-PO) composite was 3:1, which was a stable value obtained by mass monitoring for a long period of time when the GPE was pressed under a load of 9.8 N cm^{-2} using a pneumatic flat press. We also analyzed the thermal stability of electrolytes using a thermogravimetric analyzer (TGA; PerkinElmer TGA 7). The TGA experiments were conducted by heating the samples (approximately 4 mg) from room temperature to 600 °C at 5 °C min^{-1} under an N$_2$ environment.

2.2. Electrode Preparation and Cell Assembly. The cathode consisted of 80 wt % LiFePO$_4$ (BTR New Energy Materials), 10 wt % PVDF (M_w = 534 000 g mol^{-1}; Aldrich), and 10 wt % super-P (Taiwan Maxwave Co., Taiwan). A slurry of these materials was prepared in N-methyl pyrrolidone (NMP, Aldrich) and was used to coat Al foil using a blade. After solvent evaporation, 1.327 cm^2 disks as cathodes were obtained from punching the coated foil and dried at 80 °C under vacuum for 12 h. The cathodes were roll-pressed to improve particulate contact and foil adhesion. Electrode thickness ranged from 40 to 50 μm after roll-pressing, and the resulting apparent density of the electrode was 1.16 g cm^{-3}. Li/LiFePO$_4$ batteries were assembled by sandwiching the GPEs between a lithium-metal disk anode and the LiFePO$_4$ cathode. The cell was then enclosed in a coin cell and vacuum sealed to form a battery. All battery assemblies were conducted in a glovebox filled with argon gas.

2.3. Measurements. The surface morphology of the Celgard membrane and GPE was examined using a scanning electron microscope (SEM) (JEOL JSM-6700F). Fourier transform infrared spectroscopy (FTIR) in diffuse reflectance mode was conducted to analyze the functionalities of the membrane and GPE using a Jasco FTIR-4100 spectrometer. The GPE was analyzed by ac impedance spectroscopy (Zahner-Elecktrik IM6e) by inserting it between two stainless steel (SS) electrodes to determine its ionic conductivity at temperatures from −20 to 90 °C. This measurement was conducted at 0 V with an ac potential amplitude of 5 mV and a frequency range of 0.1 Hz to 1 MHz. The interface resistance (R_{int}) between the GPE and lithium-metal electrode was measured using the impedance response of the Li/GPE/Li cells. Linear sweep voltammetry was performed on a SS working electrode with a lithium counter electrode at a scan rate of 5 mV s^{-1}. Charge and discharge cycling tests were conducted on Li/LiFePO$_4$ batteries between 2.5 and 4 V (vs Li/Li$^+$) galvanostatically with battery test equipment (Acutech System BAT-750). All electrochemical measurements on the Li/LiFePO$_4$ batteries were conducted at 25 °C. For the purpose of comparison, the performance of the liquid electrolyte (1 M LiPF$_6$ EC/DMC/DEC solution) swelling the Celgard separator was also analyzed in the same manner as that for the GPE.

3. RESULTS AND DISCUSSION

3.1. Preparation of GPEs. PEO chains are an important component of GPE polymeric frameworks because they effectively solvate electrolytic ions and serve as a solvent gelator.[40,41] Copolymerization with PPO reduces the crystallization tendency of a PEO-based polymeric framework.[40] Blending DGEBA with PEO precursors reinforces the P(EO-co-PO) copolymer framework to improve mechanical properties.[38] Scheme 1 shows the conceptual structure of the P(EO-

Scheme 1. Conceptual Structure of the P(EO-co-PO) Framework^a

● Solvent molecule
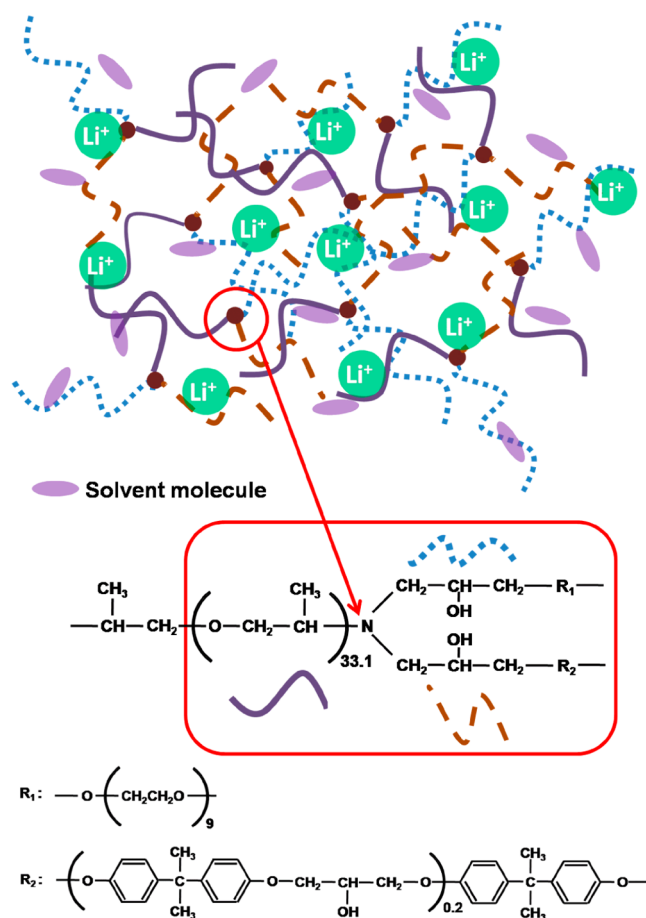
^{a}Nitrogen atoms connect the PEO, PPO, and DEGBA chains to construct a 3D network.

co-PO) framework. Nitrogen atoms connect the PEO, PPO, and DEGBA chains to construct a 3D network, which incorporates with the Celgard membrane to produce the GPE polymeric framework. The strong P(EO-co-PO) dipole moment holds solvent molecules to avoid solvent leakage or evaporation (Figure S1 of the Supporting Information), whereas Celgard assures the GPE of its mechanical integrity.

Figure 1a shows a top-view photograph of the Celgard membrane (12 μm thick) which is flexible, white, entirely opaque to light, and contains voids on the surface. After immersion in the electrolyte solution, the Celgard membrane became transparent to light (inset of Figure 1a), indicating that the solvent swelled the film by segregating the polymer-chain bundles. However, the Celgard membrane can neither trap solvent molecules nor dissociate electrolyte salts. SEM analysis (Figure 1b) shows a high concentration of voids distributed over the membrane surface. These voids increase membrane swelling and disappear after polymer swelling.

After incorporating the Celgard membrane with P(EO-co-PO) at a P(EO-co-PO) to Celgard mass ratio of 0.8:1, the resulting Celgard-P(EO-co-PO) film became transparent to light (Figure 1c) and the voids disappeared (Figure 1d). This transparency indicates that the P(EO-co-PO) chains are highly compatible with the PP and PE chains in the Celgard membrane and that they effectively segregate the polymer-chain bundles. This polymer incorporation also smeared the
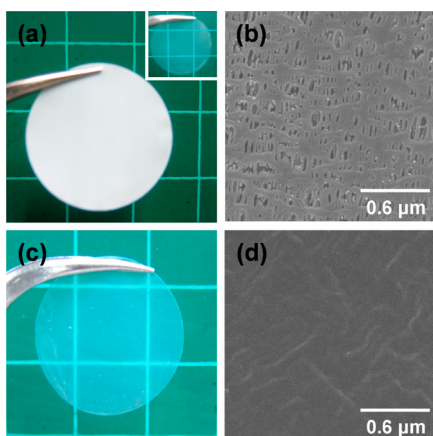
Figure 1. Top-view photographs and SEM images of the Celgard membrane (panels a and b) and the Celgard-P(EO-co-PO) film (panels c and d). The inset of panel a shows the photograph of the Celgard membrane immersed in the electrolyte solution.

Figure 3. LE-uptake behavior when soaking the Celgard-P(EO-co-PO) membrane in LE and LE-leakage behavior when pressing the LE-saturated Celgard-P(EO-co-PO) with a load of 9.8 N cm^{-2}. The LE uptake reached a saturation value of 3.3 times the membrane mass in 25 min.

membrane voids. Therefore, P(EO-co-PO) allows the composite film to trap solvent molecules to suppress solvent leakage or evaporation when it is swollen with an electrolytic solution.

An FTIR spectroscopic study was used to analyze the functional groups on the Celgard membrane and the Celgard-P(EO-co-PO) film. The Celgard spectrum in Figure 2 shows a
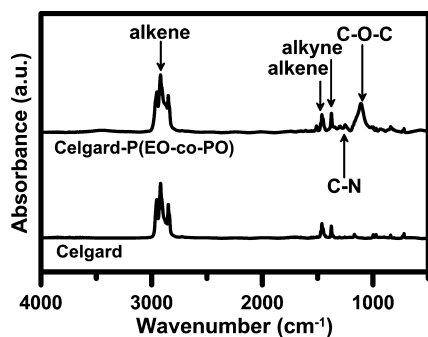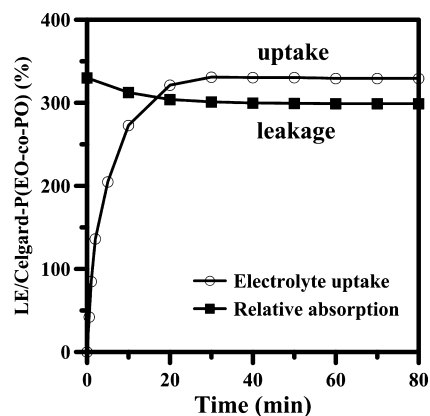

Figure 2. FTIR absorption spectra of the Celgard membrane and the Celgard-P(EO-co-PO) composite.

characteristic alkene stretching vibration near 2850 to 2960 cm^{-1}, whereas alkene and alkyne bending peaks are at 1460 and 1380 cm^{-1}, respectively.[42,43] The Celgard-P(EO-co-PO) spectrum shows additional C−O−C asymmetric stretching vibration peaks at 1110 cm^{-1} and C−N stretching vibration peaks at 1260 and 1310 cm^{-1}.[44−46] The FTIR analysis indicates that the P(EO-co-PO) copolymer did not chemically interact with the Celgard membrane, but the copolymer must have effectively segregated the Celgard polymer-chain bundles for high transparency (Figure 1c).

This study synthesized GPE by swelling the Celgard-P(EO-co-PO) composite film with a liquid electrolyte (LE) consisting of the EC/DMC/DEC solution dissolved in 1 M LiPF$_6$. Figure 3 shows the electrolyte uptake of the Celgard-P(EO-co-PO) membrane as a function of the soaking time. The membrane effectively absorbed the 1 M LiPF$_6$ LE and reached a saturation value of 3.3 times the membrane mass in 25 min. Figure 3 also shows the leakage behavior of the LE-saturated Celgard-P(EO-co-PO) membrane that was subjected to a pressing load of 9.8 N cm^{-1}. The leakage loss stabilized in 60 min, and the absorbed

amount was maintained at approximately 3 times the Celgard-P(EO-co-PO) mass. We used this stabilized LE-saturated Celgard-P(EO-co-PO) membrane as the GPE for the subsequent analysis and cell assembly. A TGA analysis shows that this GPE remained stable at temperatures as high as 100 °C (Figure S1 of the Supporting Information). A previous study reported a GPE with a stabilized LE capacity of only 1.65 times its electrospun polymer mass.[47] The superiority of the Celgard-P(EO-co-PO) membrane in holding LE may render high ionic conductivity to the resulting GPE even at low temperatures.

3.2. Ionic Conductivity. The ac impedance method was used to analyze the ionic conductivity of the GPE at various temperatures. The performance of the LE swelling the Celgard membrane as a separator was also analyzed. Figure 4a,b shows the GPE and LE impedance data at temperatures ranging from 20 to 90 °C. The less-inclined GPE spectra indicate that the GPE is more compatible with the SS electrode for facile charge transport to build up double layer at the electrode interface than the LE. The ionic conductivity of the electrolytes was determined using

$$\sigma = R_I^{-1}S^{-1}d \qquad (1)$$

where σ represents ionic conductivity, R_I is the intercept at the real axis in the impedance Nyquist plot, S is the geometric area of the electrolyte−electrode interface, and d is the distance between the two electrodes.[48]

Figure 4c shows a summary of the GPE and LE ionic conductivities at temperatures between −20 and 90 °C in the Arrhenius expression. GPE conductivity is higher than LE conductivity. For example, ionic conductivity values of 2.8×10^{-3} and 7.1×10^{-4} S cm^{-1} were obtained at 30 °C for the GPE and LE, respectively. The lower conductivity of LE is attributable to the use of the Celgard membrane separator with resistance inherent in the electrolyte system.[49] LE alone in the liquid state (that is, in the absence of a separator membrane) appears to have conductivities slightly higher than those of GPE (Figure S2 of the Supporting Information). Previous studies reported ionic conductivities of 1.1×10^{-5} S cm^{-1} for a 1 M LiPF$_6$ EC/DMC/DEC (1:1:1 by volume) solution at 20 °C and $\sim 9 \times 10^{-4}$ S cm^{-1} for 1 M LiPF$_6$ EC/EMC (3:7 by volume) at room temperature when the solutions swelled a

8480

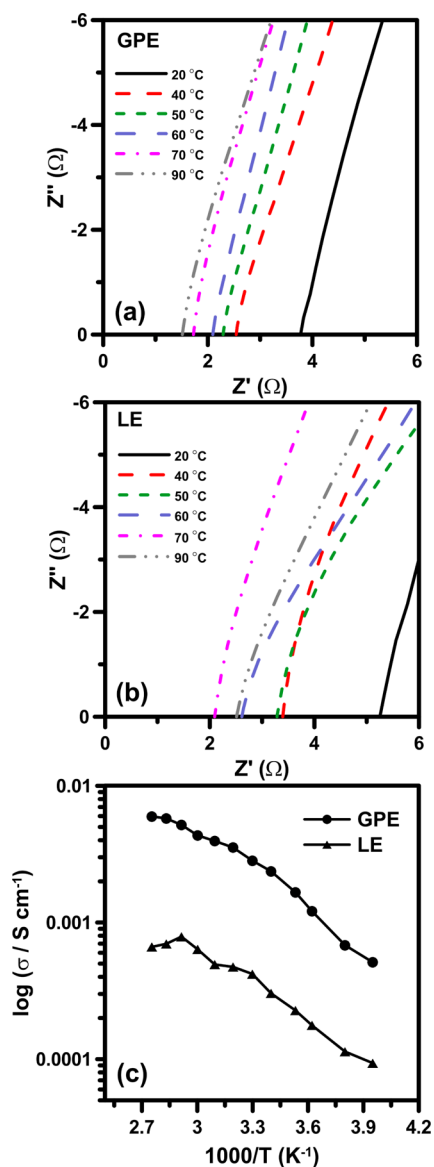dx.doi.org/10.1021/am4019115 | ACS Appl. Mater. Interfaces 2013, 5, 8477−8485

Figure 4. Nyquist impedance plots of (a) GPE and (b) LE inserted between two stainless steel electrodes with a frequency range of 0.1 Hz to 1 MHz at 0 V and temperatures of 20 to 90 °C. Panel c shows the ionic conductivities of the GPE and LE determined from the impedance data at temperatures of −20 to 90 °C.

of the polymer. Meanwhile, the solvent molecules are extensively distributed on the segregated Celgard chains and form solvent channels for ion motion. The activation energy for ion transport in the GPE and LE are similar (18 kJ mol⁻¹, Figure 4c), indicating that transport through the free volume governs GPE ionic conductivity.

Figure 4c shows that LE conductivity decreased above 80 °C. This conductivity decrease might be because at this temperature the solvent in the Celgard membrane evaporated and interfered with ionic transport in the LE phase. By contrast, GPE conductivity steadily increased with temperature and was reversible with temperature variation, indicating that incorporation with the P(EO-co-PO) polymer reinforces the solvent-holding of the Celgard framework and that the resulting GPE is more thermally stable than the LE swelling the Celgard membrane.

3.3. Electrochemical Stability. Figure 5 shows the linear scan voltammograms of cells assembled by inserting an
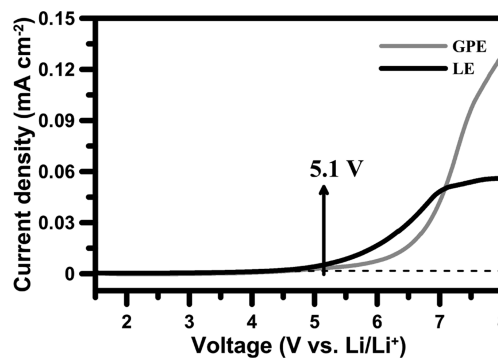

Figure 5. Linear scan voltammograms of cells assembled by inserting an electrolyte (GPE or LE) between a working stainless steel electrode and Li-metal counter electrode at 5 mV s⁻¹.

electrolyte between a working SS electrode and a Li counter electrode. While imposing anodic polarization on the working SS electrode, the LE exhibited an electrochemical stability range of 4.7 V, whereas the GPE produced a larger range of 5.1 V. Because the P(EO-co-PO) polymer improves lithium salt dissociation and solvent molecule cluster segregation, the GPE composite has a higher dielectric constant and therefore a larger stability range. The high anodic stability of the GPE makes it compatible with high-voltage cathode materials such as LiFePO$_4$, LiCoO$_2$, and LiMn$_2$O$_4$.[22]

Lithium-ion conducting polymer electrolytes generally produce a high interfacial resistance with lithium metal because of passivation layer formation.[56−58] This interfacial resistance often increases with time.[56,57] The electrolyte/Li-metal interface was analyzed with ac impedance using sandwich-type Li/electrolyte/Li cells. Figure 6a,b shows the impedance Nyquist spectra for the cells sandwiching the GPE and LE measured at various storage times. The spectra mainly consist of a semicircle with its diameter increasing with time. The inset of Figure 6a presents an equivalent circuit model that simulates the bulk solution resistance (R_b), interface resistance (R_{int}), interface capacitance (C_{int}), and Warburg impedance (Z_w) elements of the cells.[59] The real axis intercept in the high-frequency spectrum region corresponds to the R_b value, whereas the distance between the semicircle intercepts on the real axis corresponds to R_{int}, which is associated with the charge-transfer reaction, $Li^+ + e^- = Li$. Passivation film formation on the

membrane of Celgard 2320 (20 μm).[47,49] The dielectric constants of the carbonate solvents are not high enough to effectively solvate ion pairs for swift ion motion.[50] The P(EO-co-PO) copolymer chains in the GPE must have played a role in solvating the ion salt to increase the ionic conductivity.[51,52]

GPE ion conduction may occur through the free volume phase in the polymeric framework or through the swollen polymer-chain phase.[53,54] High GPE conductivity is caused by the high degree of LiPF$_6$ dissociation by P(EO-co-PO) and the segregated Celgard framework, which forms more ionic-transport channels after swelling by absorbing liquid electrolyte to a high degree.[3,31,47,55] The Li⁺ ions within the polymer network are solvated by the ether-oxygen and amine-nitrogen atoms because of their high donicity, and the dissociated PF$_6^-$ ions form hydrogen bonds with the hydroxyl groups.[38,51] The solvent molecules reduce the Li⁺ complexation degree with the oxygen and nitrogen atoms, increasing the segmental mobility
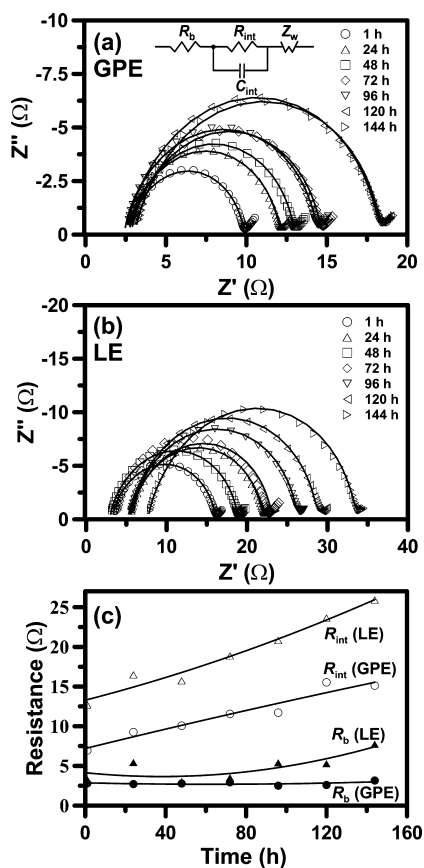
Figure 6. Nyquist impedance plots of different electrolytes using the sandwich-type Li/electrolyte/Li cell. (a) GPE and (b) LE. The inset in panel a shows the equivalent circuit used for fitting the impedance data, where R_b is the bulk solution resistance, R_{int} is the interface resistance, C_{int} is the interface capacitance, and Z_w is the Warburg impedance element. Panel c shows a summary of the R_b and R_{int} element quantities of the two cells. The measurements were performed with a frequency range of 0.1 Hz to 1 MHz at 0 V and 25 °C.

lithium-electrode surface from the electrolyte reaction increases R_{int}.[57]

Figure 6c shows a summary of the R_b and R_{int} element quantities of the two cells. The GPE cell produced smaller R_b values than the LE cell. This corresponds with the conductivity measurements in Figure 4. The R_{int} value of the LE cell was significantly larger than that of the GPE cell immediately after cell assembly (at a storage time of 1 h). Both electrolytes showed steady R_{int} increases with time. The R_{int} value of the GPE was stabilized after 120 h but that of the LE continued to increase steadily. The stabilized R_{int} of the GPE was 15 Ω, much lower than the previously reported values for gel-type electrolytes (Table 1). The larger LE R_{int} value reflects a denser coverage of the passivation layer, which was observable on the lithium-electrode surface of the LE cell. The passivation-layer growth may have resulted in the R_b increase with time when the layer was sufficiently thick to hinder ion transport to the lithium-electrode surface. By contrast, the R_b value of the GPE showed little variation with time. The low GPE R_b and R_{int} values are beneficial for electrolytes used in lithium batteries.

These results were used to develop a model explaining how polymer chains affect the charge-transfer process at the electrode/electrolyte interface. When lithium metal decomposes the carbonate solvent molecules that form solvated

cations with Li$^+$, a surface layer (a solid-electrolyte interphase (SEI) layer) forms on the lithium-metal electrode. The presence of this interfacial layer affects Li$^+$ ion movement at the interface. In the GPE cell system, the polymer network can replace carbonate molecules to solvate Li$^+$ ions with ether-oxygen and amine-nitrogen atoms on the P(EO-co-PO) chains, retarding the interaction of carbonate with lithium metal and suppressing SEI formation. A thinner SEI layer in the GPE system causes the smaller R_{int} value (relative to that in the LE) and an R_b value that does not change with storage time.

In addition to lithium ions, counteranions migrate within the electrolyte and polarize the electrodes. A stationary anion situation ($t_{Li+} = 1$) is beneficial in eliminating polarization resistance. Electrolyte t_{Li+} values were determined using dc polarization of a sandwich-type cell and ac impedance spectroscopic analysis.[60] This required applying a low dc voltage of 5 mV to the cell (Figure 7a) and measuring the initial
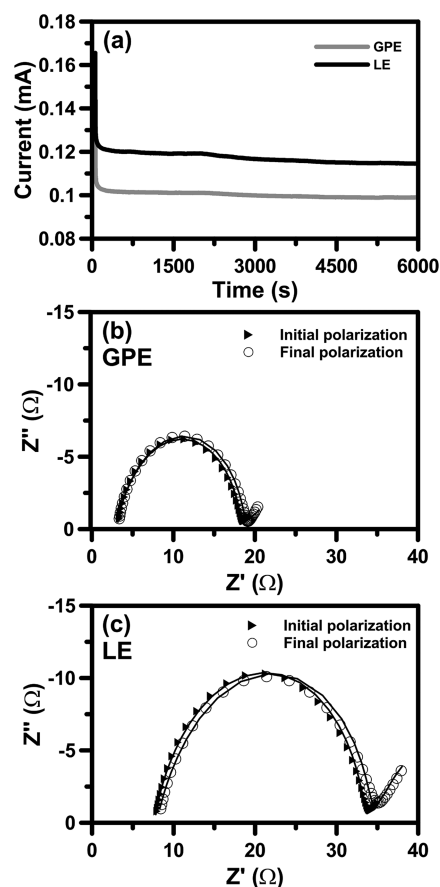

Figure 7. (a) Current−time curves of the Li/GPE/Li and Li/LE/Li cells after applying a dc voltage of 5 mV to the cell. Corresponding Nyquist impedance plots of the cells for determining the initial and final R_{int} values for (b) GPE and (c) LE.

and steady-state currents (I_0 and I_{ss}). Simultaneous ac impedance analysis monitored the initial and final resistances ($R_{int,0}$ and $R_{int,ss}$) associated with charge transfer at the Li-metal interfaces (Figure 7b,c). Polarization causes the difference between $R_{int,0}$ and $R_{int,ss}$. Combining the obtained parameters produces the t_{Li+} values.

$$t_{Li^+} = \frac{I_{ss}(\Delta V - I_0 R_{int,0})}{I_0(\Delta V - I_{ss} R_{int,ss})} \quad (2)$$

8482

dx.doi.org/10.1021/am4019115 | *ACS Appl. Mater. Interfaces* 2013, 5, 8477−8485

Using eq 2, a t_{Li+} value of approximately 0.5 was obtained for the GPE. This is much higher than 0.35 for the LE. The t_{Li+} difference indicates that P(EO-co-PO) polymer chains strongly solvate anions and hinder their motion in the solvent channels. A high t_{Li+} value decreases the electrode polarization caused by anion accumulation and suppresses the concentration gradient to facilitate lithium-ion transport. Moderated anion accumulation also improves the long-term cell cyclability.[61−63]

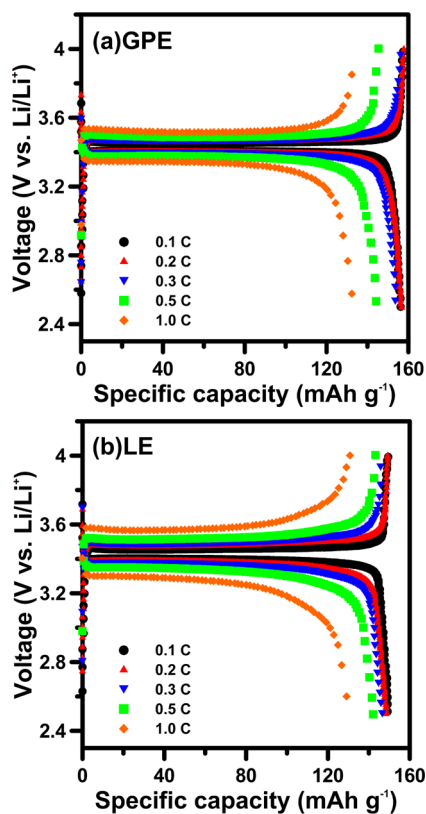**3.4. Battery Performance.** Figure 8 shows the galvanostatic charge−discharge profiles of lithium-ion batteries

Figure 8. Galvanostatic charge−discharge profiles of (a) Li/GPE/LiFePO$_4$ and (b) Li/LE/LiFePO$_4$ batteries at various C-rates between 2.5 and 4.0 V (vs Li$^+$/Li). This study assumes a maximal theoretical capacity of 170 mAh g^{-1} for the LiFePO$_4$ electrode.

assembled by inserting GPE or LE between a lithium-metal anode and a LiFePO$_4$ cathode. The battery cells were charged to 4.0 V and then discharged to 2.5 V. At low charge and discharge rates, both cells showed a voltage plateau near 3.45 V (vs Li/Li$^+$), which is typical of the biphasic Li$^+$ extraction/insertion mechanism in the LiFePO$_4$ cathode. The voltage plateau changed from 3.45 V (vs Li/Li$^+$) as the rates increased. The distinct deviation shown by the Li/LE/LiFePO$_4$ battery (Figure 8b) indicates a high battery resistance.

Figure 9 shows the voltage deviation from 3.45 V (vs Li/Li$^+$) (i.e., ΔV) for charge and discharge at various rates. The ΔV as a function of the current value shows a straight-line relationship. The intercept of the straight lines at the ordinate axis corresponds to the charge-transport overpotential in the LiFePO$_4$ particles. Because the transport processes are similar, the charge and discharge intercept values were similar (at approximately 18 mV) for both batteries.

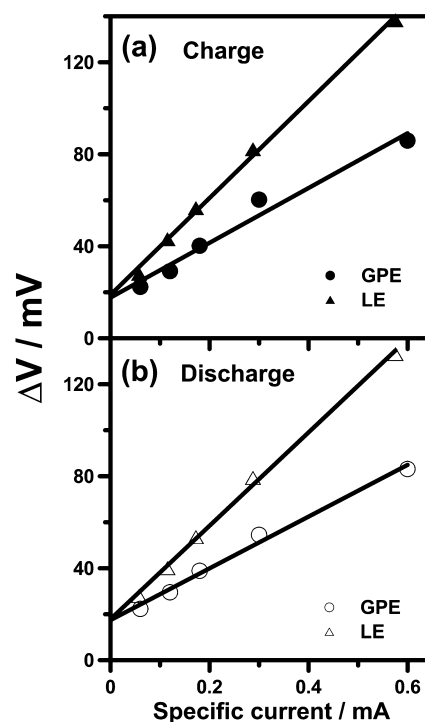The voltage value obtained by subtracting the charge-transport overpotential from the ΔV corresponds to the

Figure 9. Voltage deviation from 3.45 V (vs Li/Li$^+$) (i.e., ΔV) at various charge and discharge rates for the Li/GPE/LiFePO$_4$ and Li/LE/LiFePO$_4$ batteries. The ΔV value in the linear region corresponds to the battery's IR drop.

battery's IR drop, which has a linear relationship with current. The IR drop of the Li/GPE/LiFePO$_4$ battery was 44% smaller than that of the Li/LE/LiFePO$_4$ battery, indicating a lower energy loss in charge storage for the GPE battery. The slope of this linear relationship reflects the battery's total resistance. The straight lines in Figure 9 show that the total resistance values are similar for the charge and discharge of each battery with 117 and 206 Ω for the GPE and LE batteries, respectively. Because the R_b and R_{int} values are small relative to the total resistance values, the charge-transfer resistance in the LiFePO$_4$ electrode was the dominant factor that affected battery rate capability. The total resistance values indicate that the GPE was more efficient at charge transfer with the LiFePO$_4$ cathode than the LE. The improved efficiency of the GPE battery may be caused by the larger t_{Li+} value, which suppresses the polarization overpotential of an electrode.

This study defined the battery C-rates by assuming that the LiFePO$_4$ electrode has a maximal theoretical capacity of 170 mAh g^{-1}. Table 2 shows a summary of the battery-discharge capacities operating at various C-rates on the basis of the data in Figure 8. The GPE cell produced a high discharge capacity of 156 mAh g^{-1} at 0.1 and 0.2 C. Even at a high rate of 1 C, the battery showed a high discharge capacity of 135 mAh g^{-1}. By contrast, the LE battery produced a lower discharge capacity than that of the GPE battery. Figure 10 compares the

Table 2. Battery Discharge Capacities of Li/GPE/LiFePO$_4$ and Li/LE/LiFePO$_4$ Operating at Various C-Rates on the Basis of the Data in Figure 8

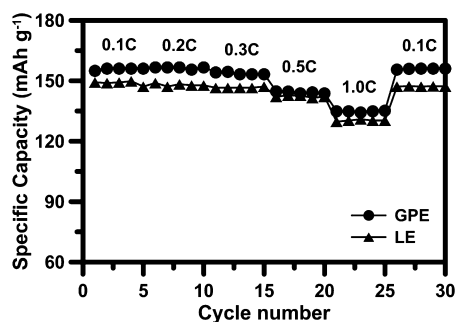| C-rates	0.1 C	0.2 C	0.3 C	0.5 C	1 C
GPE	156	156	154	145	135
LE	149	148	147	141	130

Figure 10. Discharge capacities of the Li/GPE/LiFePO₄ and Li/LE/LiFePO₄ batteries in a series of galvanostatic charge−discharge cycles at various C-rates.

discharge-capacity variations between the GPE and LE batteries in a series of galvanostatic charge−discharge cycles at various C-rates. The GPE battery outperformed the LE with a higher discharge capacity at each C-rate. Additionally, Figure 8 shows that the Li/LE/LiFePO₄ battery was charged at higher voltages and discharged at lower voltages relative to those for the Li/GPE/LiFePO₄ battery. The LE swelling Celgard led to a significant energy loss during battery operation. Incorporating the copolymer into the Celgard membrane is beneficial in reducing energy loss during charge storage. The improved GPE cell performance is caused by the strong solvation ability and a high t_{Li+} value of the GPE. In addition to its high capacity and low energy loss, the GPE battery also showed promising capacity reversibility with a negligible decay after 30 cycles of galvanostatic charge−discharge at various C-rates (Figure 10).

Figure 11 shows charge and discharge capacities as a function of the number of galvanostatic cycles at 0.5 C. The GPE cell
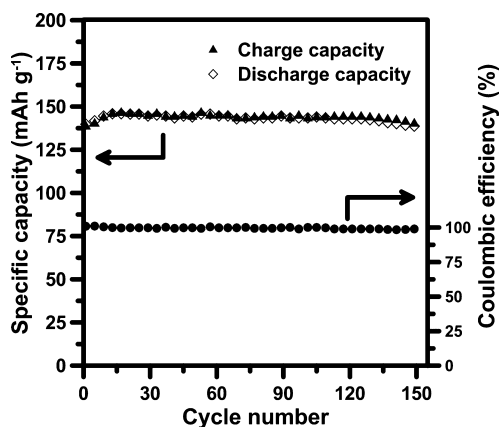

Figure 11. Charge and discharge capacities and Coulombic efficiency of the Li/GPE/LiFePO₄ battery as a function of the cycle number at 0.5 C with a voltage range between 2.5 and 4.0 V.

showed good cycling performance with a small capacity decrease of 1.2% in 150 cycles. The Coulombic efficiency, which is defined as the capacity ratio of discharge to charge, was maintained above 99% throughout the cycling process. This high Coulombic efficiency reflects high charge-transfer reversibility at the LiFePO₄/GPE interface.

4. SUMMARY AND CONCLUSIONS

This study develops a method of synthesizing a GPE by incorporating P(EO-co-PO) with a commercial Celgard membrane and swelling an LE of 1 M LiPF₆ in EC/DMC/

DEC. The P(EO-co-PO) was highly compatible with Celgard and segregated the Celgard polymer chains. The proposed GPE showed higher ionic conductivity than the LE swelling the Celgard membrane at temperatures of −20 to 90 °C. This GPE stably held LE approximately 3 times the Celgard-P(EO-co-PO) composite by mass. Ion transport was activated in the GPE and LE at 18 kJ mol^{-1}, indicating that ionic motion in the solvent channels control ion transport in the GPE. The strong solvation power of P(EO-co-PO) causes the high ionic conductivity of the GPE. The GPE showed less interfacial resistance with lithium metal than the LE. The solvation of lithium ions by the P(EO-co-PO) polymer chains may have suppressed SEI-layer formation, facilitating interfacial ion transport. The GPE had a higher Li$^+$ ion transference number than the LE (0.50 vs 0.35). This decreased the charge-transfer resistance at the LiFePO₄ surface for batteries assembled with the GPE. Because the GPE has these superior properties, the Li/GPE/LiFePO₄ battery delivered a discharge capacity of 156 and 135 mAh g^{-1} at 0.1 and 1 C, respectively (assuming a theoretical value of 170 mAh g^{-1}). It outperformed the Li/LE/LiFePO₄ battery with an approximately 5% higher charge capacity and 44% smaller IR drop. In addition, galvanostatic charge−discharge cycle measurements showed that the GPE battery lost only 1.2% of its capacity after 150 cycles. The GPE provides high storage capacity and low resistive loss and can be readily produced at an industrial level.

■ ASSOCIATED CONTENT

Ⓢ Supporting Information

Thermogravimetric analysis of GPE and LE and ionic conductivities of LE alone in the liquid state. This material is available free of charge via the Internet at http://pubs.acs.org.

■ AUTHOR INFORMATION

Corresponding Author

*E-mail: hteng@mail.ncku.edu.tw. Fax: 886-6-2344496. Tel: 886-6-2385371.

Notes

The authors declare no competing financial interest.

■ ACKNOWLEDGMENTS

■ REFERENCES

(1) Chan, C. K.; Patel, R. N.; O'Connell, M. J.; Korgel, B. A.; Cui, Y. *ACS Nano* **2010**, *4*, 1443−1450.
(2) Zhou, Y.; Kim, Y.; Jo, C.; Lee, J.; Lee, C. W.; Yoon, S. *Chem. Commun.* **2011**, *47*, 4944−4946.
(3) Huang, C. W.; Wu, C. A.; Hou, S. S.; Kuo, P. L.; Hsieh, C. T.; Teng, H. *Adv. Funct. Mater.* **2012**, *22*, 4677−4685.
(4) Huang, C. W.; Hsieh, C. T.; Kuo, P. L.; Teng, H. *J. Mater. Chem.* **2012**, *22*, 7314−7322.
(5) Xi, J.; Qiu, X.; Li, J.; Tang, X.; Zhu, W.; Chen, L. *J. Power Sources* **2006**, *157*, 501−506.
(6) Yella, A.; Lee, H. W.; Tsao, H. N.; Yi, C.; Chandiran, A. K.; Nazeeruddin, M. K.; Diau, E. W. G.; Yeh, C. Y.; Zakeeruddin, S. M.; Grätzel, M. *Science* **2011**, *334*, 629−634.
(7) Hsiao, P. T.; Liou, Y. J.; Teng, H. *J. Phys. Chem. C* **2011**, *115*, 15018−15024.

(8) Liou, Y. J.; Hsiao, P. T.; Chen, L. C.; Chu, Y. Y.; Teng, H. *J. Phys. Chem. C* **2011**, *115*, 25580−25589.

(9) Stephan, M. *Eur. Polym. J.* **2006**, *42*, 21−42.

(10) Ishikawa, M.; Morita, M.; Ihara, M.; Matsuda, Y. *J. Electrochem. Soc.* **1994**, *141*, 1730−1735.

(11) Ishikawa, M.; Ihara, M.; Morita, M.; Matsuda, Y. *Electrochim. Acta* **1995**, *40*, 2217−2222.

(12) Fergus, J. W. *J. Power Sources* **2010**, *195*, 4554−4569.

(13) Scrosati, B.; Garche, J. *J. Power Sources* **2010**, *195*, 2419−2430.

(14) Zaghib, K.; Charest, P.; Guerfi, A.; Shim, J.; Perrier, M.; Striebel, K. *J. Power Sources* **2004**, *134*, 124−129.

(15) Hwang, S. S.; Cho, C. G.; Kim, H. *Electrochem. Commun.* **2010**, *12*, 916−919.

(16) Yang, C. M.; Kim, H. S.; Na, B. K.; Kum, K. S.; Cho, B. W. *J. Power Sources* **2006**, *156*, 574−580.

(17) Li, H.; Chen, Y. M.; Ma, X. T.; Shi, J. L.; Zhu, B. K.; Zhu, L. P. *J. Membr. Sci.* **2011**, *379*, 397−402.

(18) Wang, X. L.; Cai, Q.; Fan, L. Z.; Hua, T.; Lin, Y. H.; Nan, C. W. *Electrochim. Acta* **2008**, *53*, 8001−8007.

(19) Pandey, G. P.; Agrawal, R. C.; Hashmi, S. A. *J. Power Sources* **2009**, *190*, 563−572.

(20) Ferrari, S.; Quartarone, E.; Mustarelli, P.; Magistris, A.; Fagnoni, M.; Protti, S.; Gerbaldi, C.; Spinella, A. *J. Power Sources* **2010**, *195*, 559−566.

(21) Wu, N.; Cao, Q.; Wang, X.; Li, X.; Deng, H. *J. Power Sources* **2011**, *196*, 8638−8643.

(22) Raghavan, P.; Manuel, J.; Zhao, X.; Kim, D. S.; Ahn, J. H.; Nah, C. *J. Power Sources* **2011**, *196*, 6742−6749.

(23) Kumar, D.; Hashmi, S. A. *J. Power Sources* **2010**, *195*, 5101−5108.

(24) Wang, Y.; Ma, X.; Zhang, Q.; Tian, N. *J. Membr. Sci.* **2010**, *349*, 279−286.

(25) Jung, H. R.; Lee, W. J. *Electrochim. Acta* **2011**, *58*, 674−680.

(26) Choi, J. W.; Cheruvally, G.; Kim, Y. H.; Kim, J. K.; Manuel, J.; Raghavan, P.; Ahn, J. H.; Kim, K. W.; Ahn, H. J.; Choi, D. S.; Song, C. E. *Solid State Ionics* **2007**, *178*, 1235−1241.

(27) Gentili, V.; Panero, S.; Reale, P.; Scrosati, B. *J. Power Sources* **2007**, *170*, 185−190.

(28) Zhong, Z.; Cao, Q.; Jing, B.; Wang, X.; Li, X.; Deng, H. *Mater. Sci. Eng., B* **2012**, *177*, 86−91.

(29) Idris, N. H.; Rahman, M. M.; Wang, J. Z.; Liu, H. K. *J. Power Sources* **2012**, *201*, 294−300.

(30) Raghavan, P.; Zhao, X.; Shin, C.; Baek, D. H.; Choi, J. W.; Manuel, J.; Heo, M. Y.; Ahn, J. H.; Nah, C. *J. Power Sources* **2008**, *195*, 6088−6094.

(31) Rao, M.; Geng, X.; Liao, Y.; Hu, S.; Li, W. *J. Membr. Sci.* **2012**, *399*, 37−42.

(32) Liao, Y.; Sun, C.; Hu, S.; Li, W. *Electrochim. Acta* **2013**, *89*, 461−468.

(33) Liu, L.; Yang, P.; Li, L.; Cui, Y.; An, M. *Electrochim. Acta* **2012**, *85*, 49−56.

(34) Li, M.; Yang, L.; Fang, S.; Dong, S.; Jin, Y.; Hirano, S. I.; Tachibana, K. *J. Power Sources* **2011**, *196*, 6502−6506.

(35) Sirisopanaporn, C.; Fernicola, A.; Scrosati, B. *J. Power Sources* **2009**, *186*, 490−495.

(36) Song, J. Y.; Wang, Y. Y.; Wan, C. C. *J. Power Sources* **1999**, *77*, 183−197.

(37) Liang, W. J.; Chen, T. Y.; Kuo, P. L. *J. Appl. Polym. Sci.* **2004**, *92*, 1264−1270.

(38) Tien, C. P.; Liang, W. J.; Kuo, P. L.; Teng, H. *Electrochim. Acta* **2008**, *53*, 4505−4511.

(39) Eo, S. M.; Cha, E.; Kim, D. W. *J. Power Sources* **2009**, *189*, 766−770.

(40) Armand, M. M. In *Polymer Electrolyte Reviews*, 1st ed.; MacCallum, J. R., Vincent, C. A., Eds.; Elsevier: London, 1987; Vol. *1*, p 1.

(41) Kang, Y.; Cheong, K.; Noh, K. A.; Lee, C.; Seung, D. Y. *J. Power Sources* **2003**, *119*, 432−437.

(42) Gulmine, J. V.; Janissek, P. R.; Heise, H. M.; Akcelrud, L. *Polym. Test.* **2002**, *21*, 557−563.

(43) He, P.; Xiao, Y.; Zhang, P.; Xing, C.; Zhu, N.; Zhua, X.; Yan, D. *Polym. Degrad. Stab.* **2005**, *88*, 473−479.

(44) Wang, R.; Jiang, X.; Yin, G.; Yin, J. *Polymer* **2011**, *52*, 368−375.

(45) Zheng, S.; Zhang, N.; Luo, X.; Ma, D. *Polymer* **1995**, *36*, 3609−3613.

(46) Deng, C.; Chen, X.; Yu, H.; Sun, J.; Lu, T.; Jing, X. *Polymer* **2007**, *48*, 139−149.

(47) Carol, P.; Ramakrishnan, P.; John, B.; Cheruvally, G. *J. Power Sources* **2011**, *196*, 10156−10162.

(48) Kuo, P. L.; Liang, W. J.; Chen, T. Y. *Polymer* **2003**, *44*, 2957−2964.

(49) Arora, P.; Zhang, Z. *Chem. Rev.* **2004**, *104*, 4419−4462.

(50) Brodd, R. J. *Chem. Rev.* **2004**, *104*, 4245−4270.

(51) Fonseca, C. P.; Cavalcante, F., Jr.; Amaral, F. A.; Souza, C. A. Z.; Neves, S. *Int. J. Electrochem. Sci.* **2007**, *2*, 52−63.

(52) Lin, C. L.; Kao, H. M.; Wu, R. R.; Kuo, P. L. *Macromolecules* **2002**, *35*, 3083−3096.

(53) Cohen, M. H.; Turnbull, D. *J. Chem. Phys.* **1959**, *31*, 1164−1169.

(54) Saunier, J.; Alloin, F.; Sanchez, J. Y.; Caillon, G. *J. Power Sources* **2003**, *119−121*, 454−459.

(55) Rao, M. M.; Liu, J. S.; Li, W. S.; Liang, Y.; Zhou, D. Y. *J. Power Sources* **2008**, *322*, 314−319.

(56) Zhang, T.; Imanishi, N.; Hasegawa, S.; Hirano, A.; Xie, J.; Takeda, Y.; Yamamoto, O.; Sammes, N. *J. Electrochem. Soc.* **2008**, *155*, A965−A9690.

(57) Appetecchi, G. B.; Croce, F.; Dautzenberg, G.; Mastragostino, M.; Ronci, F.; Scrosati, B.; Soavi, F.; Zanelli, A.; Alessandrini, F.; Prosini, P. P. *J. Electrochem. Soc.* **1998**, *145*, 4126−4132.

(58) Sun, H. Y.; Takeda, Y.; Imanishi, N.; Yamamoto, O.; Sohn, H. J. *J. Electrochem. Soc.* **2000**, *147*, 2462−2467.

(59) Liu, S.; Imanishi, N.; Zhang, T.; Hirano, A.; Takeda, Y.; Yamamoto, O.; Yang, J. *J. Electrochem. Soc.* **2010**, *157*, A1092−A1098.

(60) Evans, J.; Vincent, C. A.; Bruce, P. G. *Polymer* **1987**, *28*, 2324−2328.

(61) Dias, F. B.; Plomp, L.; Veldhuis, J. B. J. *J. Power Sources* **2000**, *88*, 169−191.

(62) Sumathipala, H. H.; Hassoun, J.; Panero, S.; Scrosati, B. *J. Appl. Electrochem.* **2008**, *38*, 39−42.

(63) Doyle, M.; Fuller, T. F.; Newman, J. *Electrochim. Acta* **1994**, *39*, 2073−2081.

8485

dx.doi.org/10.1021/am4019115 | *ACS Appl. Mater. Interfaces* 2013, 5, 8477−8485